Chinese Journal of Catalysis 37 (2016) 1721–1728

available at www.sciencedirect.com

ScienceDirect

journal homepage: www.elsevier.com/locate/chnjc

Article (Special Issue on Gold Catalysis)

Enhanced catalytic activities and selectivities in preferential oxidation of CO over ceria-promoted Au/Al_2O_3 catalysts

Yu-Xin Miao, Jing Wang, Wen-Cui Li *

State Key Laboratory of Fine Chemicals, School of Chemical Engineering, Dalian University of Technology, Dalian 116024, Liaoning, China

ARTICLE INFO

Article history:
Received 26 April 2016
Accepted 20 May 2016
Published 5 October 2016

Keywords:
Gold catalysis
Ceria
Alumina
Preferential oxidation of carbon monoxide
Deposition-precipitation

ABSTRACT

The preferential oxidation of CO (CO-PROX) is a hot topic because of its importance in proton-exchange membrane fuel cells (PEMFCs). Au catalysts are highly active in CO oxidation. However, their activities still need to be improved at the PEMFC operating temperatures of 80–120 °C. In the present study, Au nanoparticles of average size 2.6 nm supported on ceria-modified Al_2O_3 were synthesized and characterized using powder X-ray diffraction, nitrogen physisorption, transmission electron and scanning transmission electron microscopies, temperature-programmed hydrogen reduction (H_2-TPR), Raman spectroscopy, and *in situ* diffuse-reflectance infrared Fourier-transform spectroscopy. Highly dispersed Au nanoparticles and strong structures formed by Au–support interactions were the main active species on the ceria surface. The Raman and H_2-TPR results show that the improved catalytic performance of the Au catalysts can be attributed to enhanced strong metal–support interactions and the reducibility caused by ceria doping. The formation of oxygen vacancies on the catalysts increased their activities in CO-PROX. The synthesized Au catalysts gave excellent catalytic performances with high CO conversions (> 97%) and CO_2 selectivities (> 50%) in the temperature range 80–150 °C.

© 2016, Dalian Institute of Chemical Physics, Chinese Academy of Sciences.
Published by Elsevier B.V. All rights reserved.

1. Introduction

Proton-exchange membrane fuel cells (PEMFCs) have attracted much attention because of their high current densities, low operating temperatures, and long working lives [1]. However, the Pt-based anode of a PEMFC is prone to poisoning by CO at operating temperatures of 80–120 °C [2,3]. Hopcalite catalysts are generally used for CO removal. Although Cu-based catalysts have the advantages of low cost and high catalytic activities in CO oxidation [4–7], they are not suitable for use in preferential oxidation of CO (CO-PROX) in a H_2-rich stream in the presence of CO_2 and H_2O [8–10]. Au nanoparticles are popular noble-metal catalysts and are used in the water-gas shift reaction [11,12] and CO oxidation [13,14]. Au nanoparticle catalysts show excellent catalytic performance in low-temperature CO oxidation, but the catalytic activities of monometallic Au catalysts are limited to those with competitive oxidation of H_2 at 80–120 °C [15,16]. The development of effective Au catalysts with enhanced catalytic performance in CO-PROX is therefore needed.

This challenge has been addressed using Au catalysts modified with reducible oxides such as TiO_2 [17], MnO_2 [18], FeO_x [17,19], and CeO_2 [17,20]; these catalysts have potential for use in CO-PROX. Ceria is an important catalytic material in heterogeneous catalysis [21,22]. Ceria-based materials enhance catalytic activities because of the oxygen storage capacity (OSC) of

* Corresponding author. Tel/Fax: +86-411-84986355; E-mail: wencuili@dlut.edu.cn
This work was supported by the National Basic Research Program of China (973 Program, 2013CB934104) and the National Natural Science Foundation of China (21225312, U1303192).
DOI: 10.1016/S1872-2067(16)62469-5 | http://www.sciencedirect.com/science/journal/18722067 | Chin. J. Catal., Vol. 37, No. 10, October 2016

ceria, which is associated with the formation of oxygen vacancies, and the excellent Ce^{4+}/Ce^{3+} redox reaction [23]. Ceria-doped Al_2O_3 composite materials are promising three-way catalysts [24]. Yuan et al. [25] reported a uniform ceria nanocatalyst stabilized by ordered mesoporous alumina as a catalyst support for Au in CO oxidation; 100% CO conversion was achieved at room temperature. Appropriate supports such as carbon materials [26,27] and mesoporous alumina [28,29] can endow specific catalytic functions by suppressing nanoparticle agglomeration and enhancing the synergistic effects of strong metal–support interactions (SMSIs).

Recently, we reported a K-treated Au–Cu/Al_2O_3 catalyst produced using laboratory-synthesized γ-Al_2O_3 with a controlled morphology; the catalyst was active and stable in CO-PROX even in the presence of CO_2 or H_2O [30]. It was proposed that the introduction of Cu strengthens CO adsorption on the catalyst and K treatment significantly increases the stability of active Cu^+ species. Based on the above results, a series of ceria-doped Au catalysts were prepared and investigated using X-ray diffraction (XRD), transmission electron microscopy (TEM), Raman spectroscopy, temperature-programmed reduction of H_2 (H_2-TPR), and *in situ* diffuse-reflectance infrared Fourier-transform spectroscopy (DRIFTS). Ceria addition enhanced the reducibility and oxygen activation of the Au catalyst, resulting in improved CO-PROX activity.

2. Experimental

2.1. Catalyst preparation

All reagents were analytical grade and used without further purification. The alumina supports were prepared hydrothermally [31]. In a typical procedure, $KAl(SO_4)_2{\cdot}12H_2O$ (2.372 g) and $CO(NH_2)_2$ (0.601 g) were separately dissolved in 50 mL of deionized water. The two solutions were mixed and stirred for 0.5 h. The mixture was transferred to a Teflon-lined stainless-steel autoclave and hydrothermal treatment was performed at 180 °C for 3 h. After thorough centrifugation, the product was washed with deionized water and ethanol several times, dried at 80 °C overnight, and calcined at 600 °C in air for 2 h; this product is denoted by Al. A ceria-doped alumina support was prepared using an incipient wetness impregnation method, in which Al was impregnated with a aqueous solution of $Ce(NO_3)_3{\cdot}6H_2O$ (0.35 mol L^{-1}). The obtained CeO_2/Al_2O_3 composite was dried overnight at 50 °C and calcined at 500 °C for 2 h; this product is denoted by CeAl.

The Au–Cu/CeO_2–Al_2O_3 catalyst was prepared using our recently reported two-step deposition-precipitation (DP) method [30]. The required amount of $Cu(NO_3)_2{\cdot}9H_2O$ solution (0.1 mol L^{-1}) was added to an aqueous suspension of CeAl and the pH was controlled to ca. 8 by adding $(NH_4)_2CO_3$ solution (0.5 mol L^{-1}). The mixture was stirred at 60 °C for 2 h. The Cu/CeAl catalyst was obtained by centrifugation, and then washed and dried under vacuum. Au was deposited on the Cu/CeAl surface using $HAuCl_4$ solution (7.888 g L^{-1}) as the Au precursor and $(NH_4)_2CO_3$ as the precipitant, as in the first procedure described above. This sample is denoted as Au–Cu/CeAl. For comparison, Au/Al_2O_3 and Au/CeO_2–Al_2O_3 catalysts were prepared using the DP method; these are denoted by Au/Al and Au/CeAl, respectively. A K-doped Au–Cu/CeO_2–Al_2O_3 bimetallic catalyst was prepared using an incipient wetness impregnation method. Typically, the required amount of KNO_3 solution was added to Au–Cu/CeO_2–Al_2O_3 powder with mixing and then aging at room temperature for 1 h. The mixture was dried under vacuum overnight. The obtained K-doped Au–Cu/CeO_2–Al_2O_3 bimetallic catalyst is denoted by Au–Cu/K–CeAl. The Au loading on each catalyst was 1 wt%, and the K loading was fixed at 2 wt%. All the steps described above were performed under light exclusion by covering the round-bottomed flask with Al foil.

2.2. Catalyst characterization

XRD was performed using a Rigaku D/MAX-2400 diffractometer (40 kV, 100 mA) with Cu K_α radiation (λ = 1.54056 Å). Nitrogen adsorption–desorption isotherms were recorded using a Micromeritics Tristar 3000 instrument at −196 °C. The Brunauer–Emmett–Teller surface areas (S_{BET}) and pore size distributions of the prepared catalysts were calculated using the BET and Barrett–Joyner–Halenda method, respectively. The metal loadings on the catalysts were determined using inductively coupled plasma atomic emission spectroscopy (ICP-AES; Optima 2000 DV). TEM images of the Au catalysts were obtained using an FEI Tecnai G220 S-Twin microscope, at an accelerative voltage of 200 kV. High angle angular dark field scanning transmission electron microscopy (HAADF-STEM) and energy-dispersive X-ray spectroscopy (EDX) were performed using an FEI Tecnai F30 electron microscope at an accelerating voltage of 300 kV. Raman spectra were recorded using a Thermo DXR Raman microscope, at a laser excitation wavelength of 532 nm. H_2-TPR was performed using a Micromeritics Autochem II 2920 instrument equipped with a thermal conductivity detector (TCD) to detect H_2 consumption. Before each H_2-TPR test, the fresh samples were pretreated in an Ar flow at 150 °C for 30 min. After cooling to 40 °C, the gas atmosphere was switched to 8 vol% H_2/Ar at a rate of 50 mL min^{-1} and the catalyst was heated from 40 to 800 °C (10 °C min^{-1}). *In situ* DRIFTS was performed using a Nicolet 6700 FT-IR spectrometer equipped with a mercury cadmium telluride detector and a low-temperature DRIFTS cell (Harrick). Prior to each test, the catalyst was evacuated at 200 °C for 30 min and cooled to room temperature, and the background spectrum was recorded in an He flow at the desired temperature before the introduction of 5 vol% CO/He.

2.3. Catalytic activity measurements

The catalytic performance in CO-PROX was investigated using a fixed-bed flow reactor (i.d. 8 mm) at atmospheric pressure in the temperature range 30–150 °C, at which the water-gas shift reaction is negligible. The reaction temperature was controlled using a thermocouple located at the middle of the catalyst bed. The feed gas, which consisted of 1 vol% CO + 1 vol% O_2 + 40 vol% H_2, and balance N_2, was passed through 100

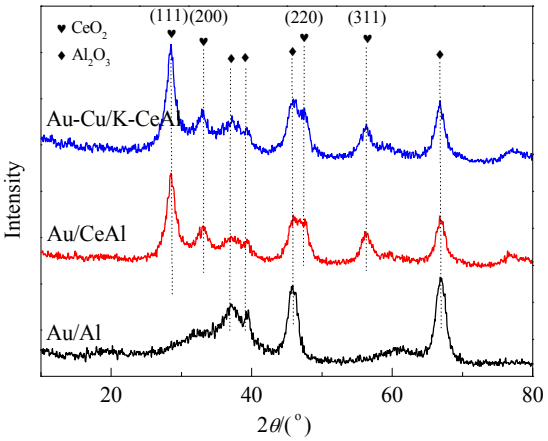

Fig. 1. XRD patterns of various Au catalysts.

mg of sample at a flow rate of 67 mL min^{-1} with a space velocity of 40 000 mL g_{cat}^{-1} h^{-1}. Prior to each measurement, the catalyst was pretreated in air at 250 °C for 2 h. The composition of the effluent gas was determined using an on-line Tianmei GC-7890 gas chromatograph equipped with a TCD. The CO conversion and CO_2 selectivity were calculated as

$$X_{CO} = ([CO]_{in} - [CO]_{out})/[CO]_{in} \times 100\%$$

$$X_{O2} = ([O_2]_{in} - [O_2]_{out})/[O_2]_{in} \times 100\%$$

$$S_{CO2} = ([CO]_{in} - [CO]_{out})/(2 \times ([O_2]_{in} - [O_2]_{out})) \times 100\%$$

where X represents the conversion of CO or O_2, and S represents the selectivity for CO oxidation by O_2.

3. Results and discussion

3.1. Catalyst characterization

Fig. 1 shows the XRD patterns of the synthesized Au/Al, Au/CeAl, and Au–Cu/K–CeAl samples. The diffraction peaks for the Au/Al sample are characteristic of crystalline γ-alumina (JCPDS 10-0425). The presence of crystalline CeO_2 particles can be observed for the ceria-doped Au/CeAl and Au–Cu/K–CeAl samples. The (111), (200), (220), and (311) diffraction peaks can be assigned to cubic CeO_2 with the fluorite structure (JCPDS 34-0394). The Au–Cu/K–CeAl diffraction peaks become broader and shift to slightly higher Bragg angles because of the incorporation of Ce ions into the alumina lattice, suggesting the formation of Ce–Al–O solid solutions. This result is similar to that in our previous work [18]. The mean ceria crystallite size (10 nm) was estimated using Scherrer's equation. No diffraction peaks for Au and Cu are observed, which indicates that the metal nanoparticles are highly dispersed on the support or the metallic loadings are low (below 5 wt%).

Table 1
Physicochemical properties of synthesized Au catalysts.

Catalyst	Loading[a] (wt%)				S_{BET}[b]	V_{total}[c]
	Au	Cu	Ce	K	(m^2 g^{-1})	(cm^3 g^{-1})
Au/Al	0.92	—	—	—	160	0.54
Au/CeAl	0.90	—	7.87	—	143	0.50
Au-Cu/CeAl	0.93	0.31	7.85	—	136	0.51
Au-Cu/K-CeAl	0.98	0.34	7.34	1.95	122	0.42

[a] The actual loadings of Au, Cu, Ce and K were determined by ICP.
[b] Specific surface area calculated by the BET method.
[c] Total pore volume at p/p_0 = 0.99.

The BET surface areas and pore size distributions of the synthesized Au catalysts were determined based on nitrogen physisorption measurements at –196 °C; the isotherms are shown in Fig. 2. All the samples show type IV isotherms with visible type H4 hysteresis loops at relative pressures (p/p_0) of 0.5–1.0, indicating the presence of slit-shaped pores (Fig. 2(a)). Fig. 2(b) shows that the samples have broad mesopore distributions. The textural properties of the catalysts are listed in Table 1. The pore structures of the Au/Al, Au/CeAl, and Au–Cu/K–CeAl catalysts were only slightly affected by doping with ceria. However, the BET surface area and total pore volume of the Au–Cu/K–CeAl catalyst decreased slightly. The experimental metal contents, obtained using ICP-AES, are in good agreement with the theoretical values (Table 1).

The morphologies and structures of the Au/CeAl and Au–Cu/K–CeAl samples were examined using TEM; the images are shown in Fig. 3. The TEM images of the Au catalyst pre-

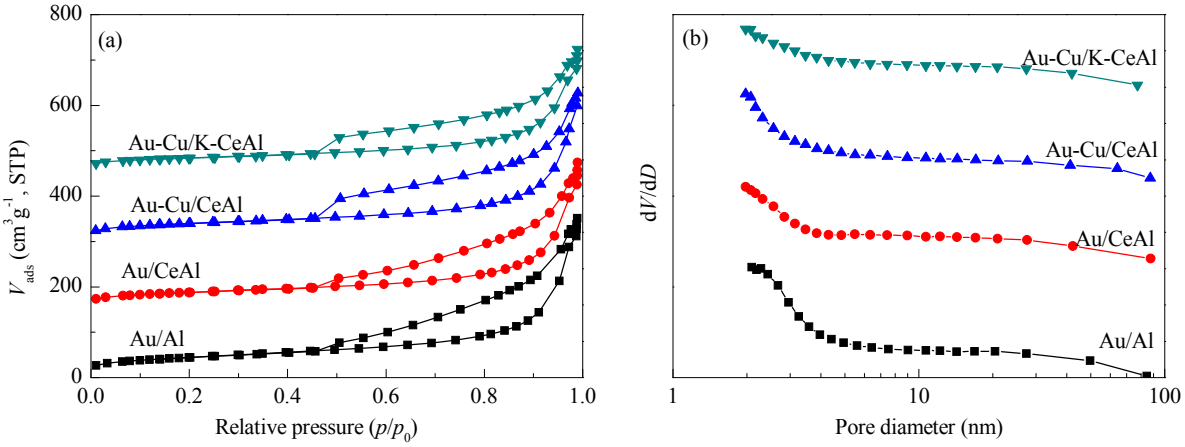

Fig. 2. Nitrogen adsorption–desorption isotherms (a) and pore size distributions (b) of Au catalysts. The Au/CeAl, Au–Cu/CeAl, and Au–Cu/K–CeAl isotherms were offset vertically by 150, 300, and 400 cm^3 g^{-1}, STP, respectively.

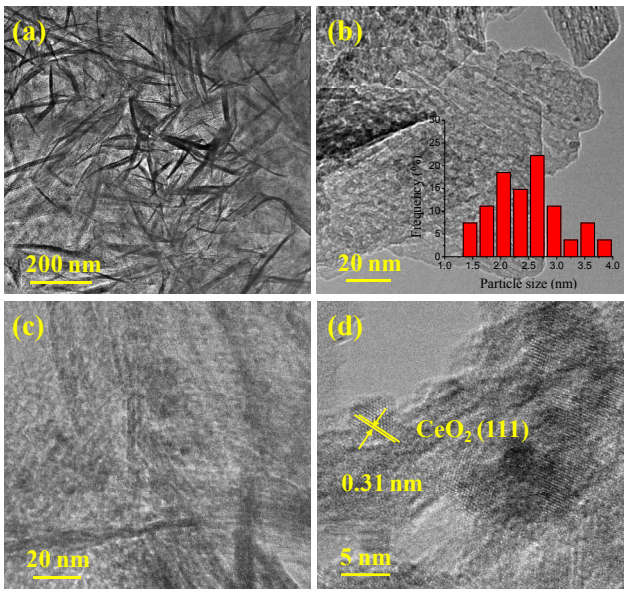

Fig. 3. TEM images of Au/CeAl (a, b) and Au–Cu/K–CeAl (c, d) catalysts.

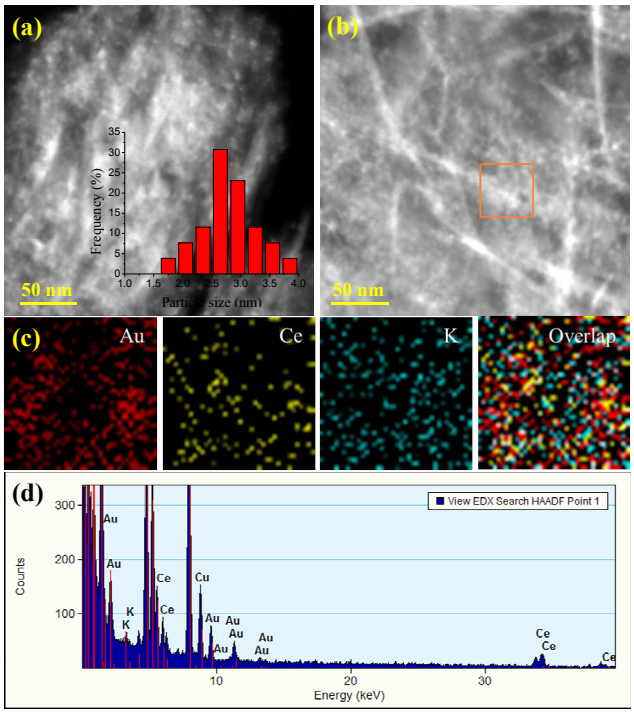

Fig. 4. HAADF-STEM images (a, b), typical EDX maps (c) based on selected area shown in (b), and EDX spectrum (d) of Au–Cu/K–CeAl catalyst.

pared on a ceria-doped Al_2O_3 support show that Au nanoparticles of size 2.4 nm were highly dispersed without aggregation (Fig. 3(a) and (b)). The low-magnification image (Fig. 3(c)) of the Au–Cu/K–CeAl sample shows that Au–Cu nanoparticles (less than 5 nm) were homogeneously dispersed on the ceria-doped Al_2O_3 support, and the particle size distribution was uniform. The high-magnification image (Fig. 3(d)) shows lattice fringes with interplanar distances of 0.31 nm, corresponding to the (111) lattice plane of a ceria solid solution. The average particle size of ceria species was ca. 8–10 nm; this is consistent with the average crystallite sizes obtained from the XRD patterns. The addition of ceria clearly changes the size, pore structure, and BET surface area of the Au/Al catalyst. The XRD, ICP-AES, and TEM results confirm that a highly dispersed Au–Cu/K–CeAl catalyst was synthesized.

The structural features of the ceria-modified Au catalysts were further investigated using HAADF-STEM. The high-magnification images (Fig. 4(a) and (b)) clearly show the microstructures of the Au–Cu/K–CeAl sample. The small Au–Cu nanoparticles were highly dispersed, with a mean size of 2.8 nm. The STEM-EDX elemental mappings (Fig. 4(c) and (d)) corresponding to the selected region in Fig. 4(b) confirm that the Au, Ce, and K species were homogeneously dispersed on the Al_2O_3 support surface over the field of view. More importantly, the Au nanoparticles tended to be supported on Ce-rich areas; this can be ascribed to enhanced SMSIs.

3.2. *Catalytic performance*

Fig. 5 shows the catalytic activities and selectivities in CO-PROX of various Au catalysts. The Au/Al catalyst had high

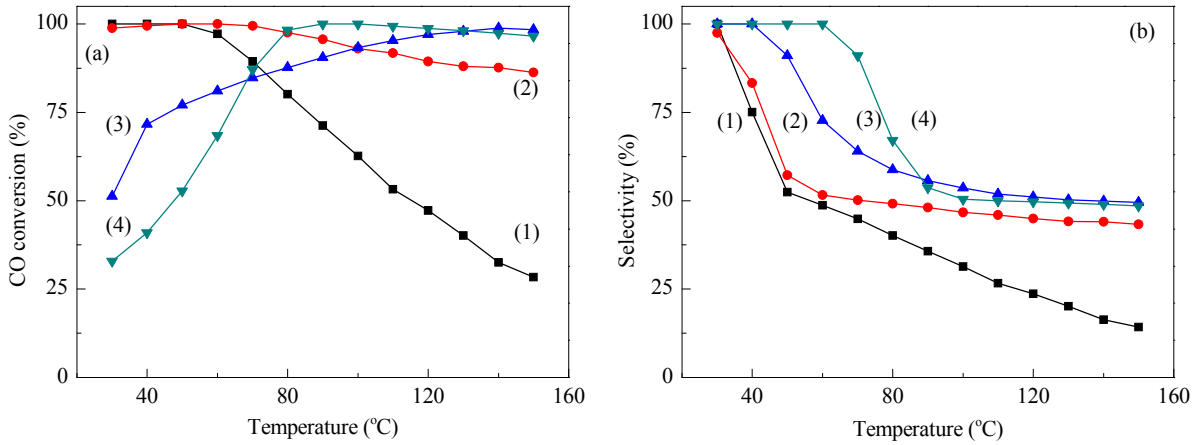

Fig. 5. CO conversions (a) and CO_2 selectivities (b) as a function of CO-PROX temperature over various Au catalysts. Reaction conditions: 1 vol% CO, 1 vol% O_2, 40 vol% H_2, and balance N_2; weight hourly space velocity 40 000 mL g_{cat}^{-1} h^{-1}. (1) Au/Al; (2) Au/CeAl; (3) Au–Cu/CeAl; (4) Au–Cu/K–CeAl.

CO oxidation activity and gave maximum CO conversion, i.e., 100% at 30–50 °C. However, the CO conversion and CO_2 selectivity decreased significantly because of H_2 oxidation when the CO-PROX temperature was increased. Ceria addition systematically increased the catalytic activity compared with that of the Au/Al sample. The Au/CeAl catalyst gave 100% CO conversion over the temperature range 30–70 °C; the conversion decreased slightly with increasing temperature and remained at approximately 86% at 150 °C. The CO_2 selectivity dropped to 50% at 70 °C, and remained stable at around 45% at the PEMFC operating temperature. The Au–Cu/CeAl and Au–Cu/K–CeAl catalysts were less active at low temperatures, but the CO conversions gradually increased with increasing temperature and reached 100% at temperatures of 140 and 90 °C, respectively. Similar trends have been reported recently for Au–Cu/Al and Au–Cu/K–Al catalysts [30]. These results show that, for CO-PROX, the Au–Cu/K–CeAl catalyst benefits from species in each active phase, i.e., Au^0 and Cu^+ species. It gives complete CO conversion at the PEMFC operating temperature, as do the Au–Cu/Al and Au–Cu/K–Al catalysts, whereas at higher reaction temperatures its catalytic behavior is similar to that of the Au–Cu/CeAl catalyst, with 100% CO conversion at 140–150 °C. Ceria addition systematically enhances the CO-PROX activity at 80–150 °C compared with those of Au/Al and Au–Cu/K–Al. To the best of our knowledge, the CO-PROX catalytic performance of the Au–Cu/K–CeAl catalyst is the highest reported to date [18].

3.3. Roles of ceria and Cu species

The ceria-modified Au catalysts were examined using Raman spectroscopy, which provides information on the extent of disordering and changes in electronic structures. The results are shown in Fig. 6(a). The spectra all show a Raman peak at 458 cm^{-1}, which can be ascribed to the strong F_{2g} mode of fluorite CeO_2. The weak peaks at ca. 567–588 cm^{-1} are associated with the presence of Ce^{3+} and indicate oxygen vacancy creation [32]. For the Au/CeAl sample, the position of the Raman F_{2g} vibration peak is similar to that reported in the literature for pure CeO_2 (461 cm^{-1}) [33]. For the Au–Cu/CeAl catalyst, the F_{2g} peak (ca. 562 cm^{-1}) is broader and less intense than those for the Au/CeAl sample; this indicates that the introduction of Cu may affect the Ce–O bond symmetry. The Raman peak near 588 cm^{-1} shifts to lower energy (567 cm^{-1}) on doping with Cu and K, i.e., for the Au–Cu/K–CeAl sample. This suggests that the strong interactions between Cu and Ce can be further enhanced by the introduction of K, which helps to improve the mobility of oxygen vacancies in ceria.

H_2-TPR was performed to clarify the relative reducibilities of the catalysts and to identify the surface oxygen species that

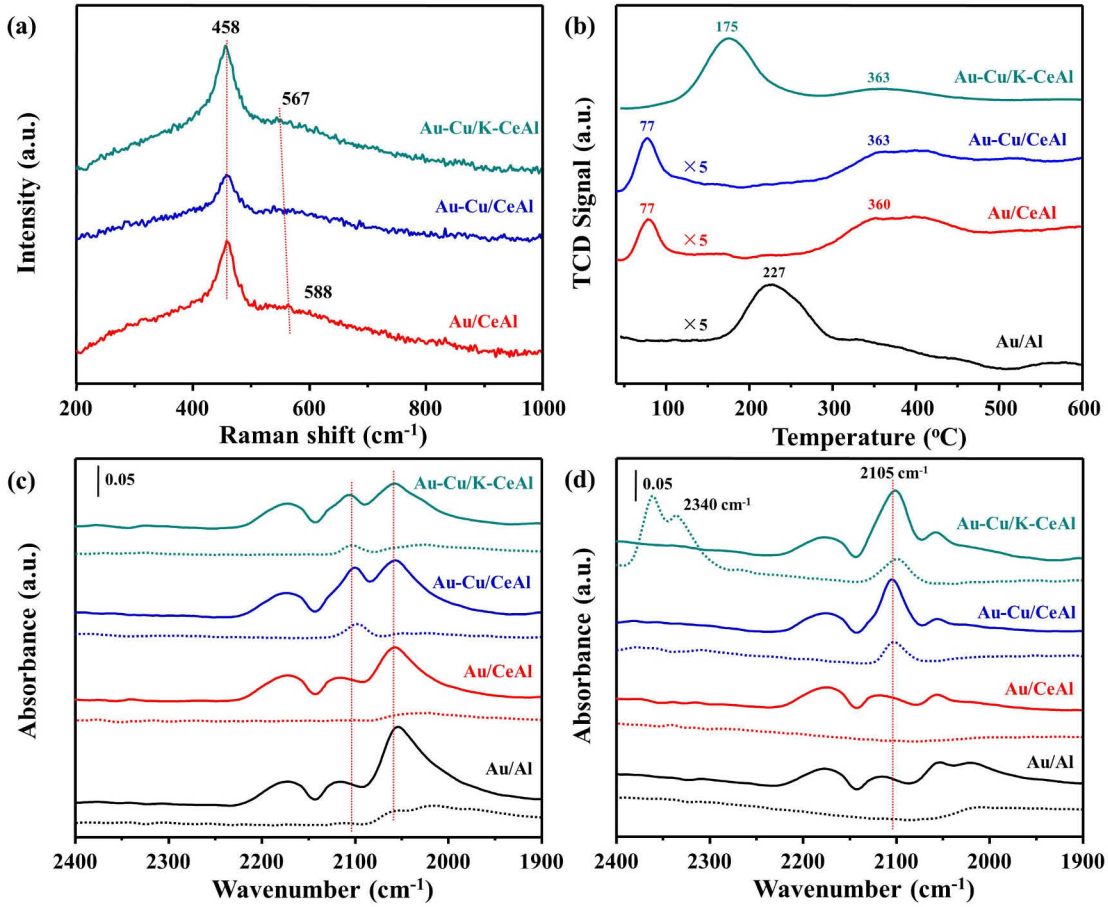

Fig. 6. Raman spectra (a) and H_2-TPR profiles (b) of various Au catalysts; DRIFT spectra of CO adsorption on various Au catalysts at 30 °C (c) and 80 °C (d); CO adsorbed for 20 min (solid line), after He purging for 10 min (dotted line).

affect the catalytic performances. Fig. 6(b) shows H_2-TPR profiles for the synthesized Au catalysts before pretreatment. The Au/Al sample shows a single peak at 227 °C corresponding to the reduction of Au_xO_y species [18]. Au/CeAl and Au–Cu/CeAl showed two similar reduction peaks, at 77 and 360 °C. The former corresponds to the reduction of surface oxygen species and Au_xO_y reduction, and the latter is associated with surface ceria reduction [34,35]. The reduction peaks of these catalysts shifted to lower temperature (77 °C) when ceria was added, indicating that the presence of ceria species improves the reducibility of surface oxygen in ceria-modified Au catalysts, possibly by promoting surface reduction of Ce^{4+} to Ce^{3+}. The formation of oxygen vacancies on the catalysts can increase the CO-PROX activity. More notably, for the Au–Cu/K–CeAl sample, the lower-temperature peak shifted to higher temperature (175 °C). This suggests that the discrepancy between the reduction peaks might be caused by enhancement of the synergetic interactions between Au and ceria species; this was confirmed using TEM and Raman.

To explain the high activity and elucidate the surface chemical properties of these Au catalysts, *in situ* DRIFTS was performed in a CO atmosphere at various adsorption temperatures. Fig. 6(c) shows the room-temperature (30 °C) DRIFT spectra of Au/CeAl, Au–Cu/CeAl, and Au–Cu/K–CeAl under CO adsorption or He-purging conditions. After CO adsorption for 20 min at 30 °C, three clear bands were observed, at 2054, 2114, and 2171 cm^{-1}, for the Au/Al sample; these are ascribed to linear adsorption of $Au^{\delta-}$–CO, Au^0–CO, and $Au^{\delta+}$–CO, respectively [31]. Similar vibration bands were observed for the Au/CeAl sample, and there were no significant differences between these and the Au/Al bands, except that the intensity of the peak at 2054 cm^{-1} was lower. This result indicates that ceria doping had little effect on CO adsorption on the Au/Al catalyst. The small Au species were highly dispersed on the support surface, and provide the main active sites for CO oxidation.

Unlike the cases for the Au/Al and Au/CeAl samples, the intensities of the peaks for linear adsorption of CO, at 2105 cm^{-1}, increased for the Au–Cu/CeAl and Au–Cu/K–CeAl samples. This suggests that the introduction of Cu strengthens CO adsorption on Au species. All these Au catalysts were purged with He after CO adsorption to confirm the conclusions based on the above analysis. For the Au/Al and Au/CeAl samples, the CO adsorption band vanished after purging for 10 min with He; this means that CO adsorption on the Au species was weak and CO was easily removed, especially at higher temperature (80 °C, Fig. 6(d)). However, CO adsorption on the Au–Cu/CeAl and Au–Cu/K–CeAl samples was stronger after purging with He, showing that Cu species strengthened CO adsorption. This conclusion is supported by the activity of Au–Cu/Al_2O_3 in CO-PROX [30].

More importantly, a new band appeared at 2340 cm^{-1}, which was ascribed to gaseous CO_2 [31]. This indicates that the CO adsorbed on Au^0 or Cu^+ readily reacts with active oxygen at 80 °C. In the Langmuir–Hinshelwood mechanism, CO adsorption and O_2 activation are key steps in CO oxidation [36]. In a previous study [30], we showed that the introduction of Cu could strengthen CO adsorption on Au–Cu/Al_2O_3 catalysts, and K treatment could significantly increase the stability of active Cu^+ species. The mobility and/or reducibility of active oxygen is therefore another important factor in CO oxidation. Active oxygen is provided by reducible oxide supports such as FeO_x and CeO_2. In our study, the TEM images show that the Au–Cu nanoparticles were homogeneously dispersed on the ceria-doped Al_2O_3 support because of the enhanced SMISs. The Raman and H_2-TPR results show that improved reducibility and formation of oxygen vacancies on the catalyst can increase the CO-PROX activity. A combination of the catalytic activity results (Fig. 5) and the results in this section suggest that the ceria component in the synthesized Au catalyst has dual roles: (1) anchoring the Au or Au–Cu nanoparticles on the alumina support and (2) providing reactive oxygen species for CO-PROX.

4. Conclusions

In this work, we showed that the incorporation of a certain amount of ceria profoundly affects the catalytic performance of supported Au/Al catalysts. Au/CeAl and Au–Cu/K–CeAl catalysts were much more active than Au/Al catalysts in CO-PROX at 80–120 °C. The synthesized Au–Cu/K–Ce–Al catalyst gave a superior catalytic performance with high CO conversion (>97%) and CO_2 selectivity (>50%) over a wide temperature range, i.e., 80–150 °C. TEM and STEM showed that highly dispersed Au and Au–Cu nanoparticles with a narrow size distribution, ranging from 1.5 to 4.0 nm, were generated on the surface of the CeAl composite support. The Au/Al sample showed lower CO-PROX activities at 80–120 °C. The Raman and H_2-TPR results suggest that ceria doping enhanced the strong interactions between Au and the composite supports and increased the reducibility of the Au–Cu/K–Ce–Al catalyst. The formation of oxygen vacancies on the ceria-modified Au catalysts strengthened the capability for oxygen activation. Overall, the results show that synergy between Au and added ceria enhances the reducibility and oxygen activation of the Au catalyst, resulting in improved CO-PROX activity. However, the specific reaction mechanism is still being explored. These results will be useful in developing other Au catalysts for heterogeneous catalysis.

References

[1] J. Wu, X. Z. Yuan, J. J. Martin, H. Wang, J. Zhang, J. Shen, S. Wu, W. Merida, *J. Power Sources*, **2008**, 184, 104–119.
[2] B. C. H. Steele, A. Heinzel, *Nature*, **2001**, 414, 345–352.
[3] T. V. Choudhary, D. W. Goodman, *Catal. Today*, **2002**, 77, 65–78.
[4] F. Yang, J. Graciani, J. Evans, P. Liu, J. Hrbek, J. F. Sanz, J. A. Rodriguez, *J. Am. Chem. Soc.*, **2011**, 133, 3444–3451.
[5] C. Y. Shiau, M. W. Ma, C. S. Chuang, *Appl. Catal. A*, **2006**, 301, 89–95.
[6] M. F. Luo, J. M. Ma, J. Q. Lu, Y. P. Song, Y. J. Wang, *J. Catal.*, **2007**, 246, 52–59.
[7] L. N. Cai, Z. H. Hu, P. Branton, W. C. Li, *Chin. J. Catal.*, **2014**, 35, 159–167.
[8] S. Scirè, C. Crisafulli, P. M. Riccobene, G. Patanè, A. Pistone, *Appl. Catal. A*, **2012**, 417–418, 66–75.

Graphical Abstract

Chin. J. Catal., 2016, 37: 1721–1728 doi: 10.1016/S1872-2067(16)62469-5

Enhanced catalytic activities and selectivities in preferential oxidation of CO over ceria-promoted Au/Al_2O_3 catalysts

Yu-Xin Miao, Jing Wang, Wen-Cui Li *
Dalian University of Technology

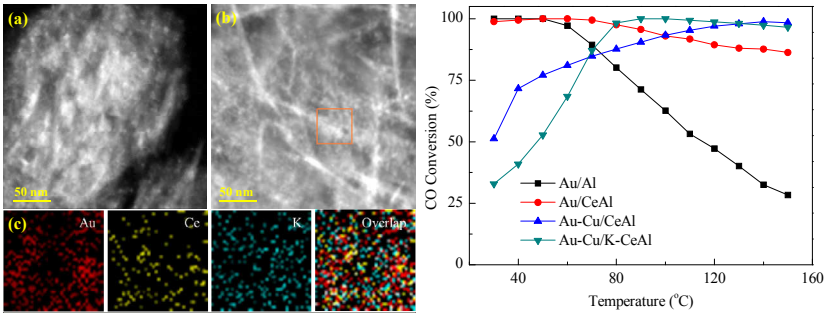

Improved synergy between Au and added ceria enhanced the reducibility and oxygen activation of an Au–Cu/K–CeAl catalyst, resulting in improved CO-PROX activity.

[9] Z. W. Wu, H. Q. Zhu, Z. F. Qin, H. Wang, J. F. Ding, L. C. Huang, J. G. Wang, *Fuel*, **2013**, 104, 41–45.
[10] A. Arango-Díaz, E. Moretti, A. Talon, L. Storaro, M. Lenarda, P. Núñez, J. Marrero-Jerezc, J. Jiménez-Jiménez, A. Jiménez-López, E. Rodríguez-Castellón, *Appl. Catal. A*, **2014**, 477, 54–63.
[11] X. Y. Liu, P. J. Guo, B. Wang, Z. Jiang, Y. Pei, K. N. Fan, M. H. Qiao, *J. Catal.*, **2013**, 300, 152–162.
[12] T. R. Reina, S. Ivanova, M. A. Centeno, J. A. Odriozola, *Appl. Catal. B*, **2016**, 187, 98–107.
[13] Y. X. Miao, L. H. Ren, L. Shi, W. C. Li, *RSC. Adv.*, **2015**, 5, 62732–62738.
[14] K. F. Zhao, H. L. Tang, B. J. Qiao, L. Li, J. H. Wang, *ACS. Catal.*, **2015**, 5, 3528–3593.
[15] P. Landon, J. Ferguson, B. E. Solsona, T. Garcia, A. F. Carley, A. A. Herzing, C. J. Kiely, S. E. Golunski, G. J. Hutchings, *Chem. Commun.*, **2005**, 3385–3387.
[16] J. A. Hernández, S. A. Gómez, T. A. Zepeda, J. C. Fierro-González, G. A. Fuentes, *ACS. Catal.*, **2015**, 5, 4003–4012.
[17] T. A. Zepeda, A. Martinez-Hernández, R. Guil-López, B. Pawelec, *Appl. Catal. B*, **2010**, 100, 450–462.
[18] Y. X. Miao, W. C. Li, Q. Sun, L. Shi, L. He, J. Wang, G. M. Deng, A. H. Lu, *Chem. Commun.*, **2015**, 51, 17728–17731.
[19] X. M. Liao, W. Chu, X. Y. Dai, V. Pitchon, *Appl. Catal. A*, **2012**, 449, 131–138.
[20] G. Avgouropoulos, M. Manzoli, F. Boccuzzi, T. Tabakova, J. Papavasiliou, T. Ioannides, V. Idakiev, *J. Catal.*, **2008**, 256, 237–247.
[21] P. J. S. Prieto, A. P. Ferreira, P. S. Haddad, D. Zanchet, J. M. C. Bueno, *J. Catal.*, **2010**, 276, 351–359.
[22] R. R. Zhang, L. H. Ren, A. H. Lu, W. C. Li, *Catal. Comm.*, **2011**, 13, 18–21.
[23] P. Venkataswamy, K. N. Rao, D. Jampaiah, B. M. Reddy, *Appl. Catal. B*, **2015**, 162, 122–132.
[24] H. Pérez-Pastenes, A. Ochoa-Tapia, T. Viveros, A. Montoya, *J. Sol-Gel Sci. Technol.*, **2006**, 37, 49–56.
[25] Q. Yuan, H. H. Duan, L. L. Li, Z. X. Li, W. T. Duan, L. S. Zhang, W. G. Song, C. H. Yan, *Adv. Mater.*, **2010**, 22, 1475–1478.
[26] Y. Hao, S. Wang, Q. Sun, L. Shi, A. H. Lu, *Chin. J. Catal.*, **2015**, 36, 612–619.
[27] Q. N. Wang, L. Shi, A. H. Lu, *ChemCatChem*, **2015**, 7, 2846–2852.
[28] J. Wang, A. H. Lu, M. R. Li, W. P. Zhang, Y. S. Chen, D. X. Tian, W. C. Li, *ACS. Nano*, **2013**, 7, 4902–4910.
[29] L. Shi, G. M. Deng, W. C. Li, S Miao, Q. N. Wang, W. P. Zhang, A. H. Lu, *Angew. Chem. Int. Ed.*, **2015**, 54, 13994–13998.
[30] Y. X. Miao, L. Shi, Q. Sun, W. C. Li, *RSC. Adv.*, **2016**, 6, 24603–24609.
[31] Y. X. Miao, L. Shi, L. N. Cai, W. C. Li, *Gold Bull.*, **2014**, 47, 275–282.
[32] O. H. Lagunaa, M. A. Centeno, G. Arzamendi, L. M. Gandía, F. Romero-Sarria, J. A. Odriozola, *Catal. Today*, **2010**, 157, 155–159.
[33] W. Y. Hernández, M. A. Centeno, F Romero-Sarria, J. A .Odriozola, *J. Phys. Chem. C*, **2009**, 113, 5629–5635.
[34] C. Pojanavaraphan, U. Satitthai, A. Luengnaruemitchai, E. Gulari, *J. Ind. Eng. Chem.*, **2015**, 22, 41–52.
[35] H. Wang, H. Q. Zhu, Z. F. Qin, F. X. Liang, G. F. Wang, J. G. Wang, *J. Catal.*, **2009**, 264, 154–162.
[36] J. Xu, Y. Q. Deng, Y. Luo, W. Mao, X. J. Yang, Y. F. Han, *J. Catal.*, **2013**, 300, 225–234.

Page numbers refer to the contents in the print version, which include both the English version and extended Chinese abstract of the paper. The online version only has the English version. The pages with the extended Chinese abstract are only available in the print version.